NMR studies of quantum chaos in a two-qubit kicked top

V. R. Krithika,[1] V. S. Anjusha,[1] Udaysinh T. Bhosale,[2] and T. S. Mahesh[1,*]

[1]*Department of Physics and NMR Research Center, Indian Institute of Science Education and Research, Pune 411008, India*

[2]*Physical Research Laboratory, Ahmedabad 380009, Gujarat, India*

(Received 14 November 2018; published 25 March 2019)

Quantum chaotic kicked top model is implemented experimentally in a two-qubit system comprising of a pair of spin-1/2 nuclei using nuclear magnetic resonance techniques. The essential nonlinear interaction was realized using indirect spin-spin coupling, while the linear kicks were realized using radio-frequency pulses. After a variable number of kicks, quantum state tomography was employed to reconstruct the single-qubit reduced density matrices, using which we could extract von Neumann entropies and Husimi distributions. These measures enabled the study of correspondence with classical phase space as well as probing distinct features of quantum chaos, such as symmetries and temporal periodicity in the two-qubit kicked top.

DOI: 10.1103/PhysRevE.99.032219

I. INTRODUCTION

Classical chaos is an extensively studied field in physics, both theoretically and experimentally. Classically chaotic systems are deterministic systems which show sensitivity to initial conditions, rendering the long-time predictions uncertain [1]. Chaos has far-reaching applications not just in physics, but in many diverse fields such as biology, chemistry, and engineering [1–3].

The correspondence principle states that classical mechanics is a limiting case of quantum mechanics, in which case, there must be some signatures of chaos in the quantum regime [4]. A direct extension of chaos to quantum mechanics is not, however, straightforward since (i) quantum dynamics is governed by the Schrödinger equation, which is linear and preserves the overlap of states, and (ii) we cannot define trajectories for quantum systems due to the constraint imposed by the uncertainty principle. A major focus of the field of quantum chaos is to understand the correspondence between quantum and classical evolutions in chaotic systems, and it has been a subject of theoretical as well as experimental interest [5–16].

The study of quantum chaos is important not only from the perspective of understanding fundamental physics, but also for applications in building operable quantum computers. For instance, it was shown that the presence of quantum chaos in a system can affect the functionality of a quantum computer [17]. Since classical measures of chaos cannot be extended to the quantum domain, quantum chaos needs to be characterized using inherent quantum mechanical properties. Signatures of quantum chaos have been studied using various quantities like entanglement [18–22], Lyapunov exponents and Husimi probability distributions [23], the dynamics of quantum discord [24], level statistics of chaotic Hamiltonians [25,26], the dynamics of open quantum systems undergoing continuous quantum measurement [27], etc. The kicked top model is a classic example for studying chaos, which shows regular to chaotic behavior as a function of the chaoticity parameter. This model has been studied theoretically [18–21,25,28–31], and also has been realized experimentally in various systems including laser-cooled cesium atoms [9] and superconducting circuits [12]. Recently, the kicked top consisting of just two qubits, which is in a deep quantum regime, has also been studied theoretically in detail [20,32]. It has been shown that the model is exactly solvable for up to four qubits [30].

In this work, we investigate quantum chaos in a two-qubit system formed by a pair of spin-1/2 nuclei using nuclear magnetic resonance (NMR) techniques. NMR has been a successful test bed to understand quantum correlations and implement various quantum information processing tasks [33,34]. It offers advantages in terms of long coherence times, precise controllability of quantum dynamics, and efficient measurement of output states. We study quantum kicked top (QKT) using spin-spin interaction between two nuclear spins as the nonlinear evolution and intermittent radio-frequency pulses as linear kicks. After a variable number of kicks, we characterize the final state via quantum state tomography. Signatures of the corresponding classical phase space are found in the time-averaged von Neumann entropy. Further analysis using Husimi probability distributions reveals contrast between regular and chaotic regions in the quantum regime.

The paper is organized as follows. Section II introduces the theory of the kicked top model. The NMR implementation, results of the experiments, and their analysis along with numerical simulations are presented in Sec. III and final conclusions are given in Sec. IV.

II. QUANTUM KICKED TOP

We now describe the use of a pair of qubits to collectively simulate a single QKT [9,25], which is described by the piecewise Hamiltonian consisting of periodic x kicks of width Δ and strength p separated by nonlinear evolutions each of an

*mahesh.ts@iiserpune.ac.in

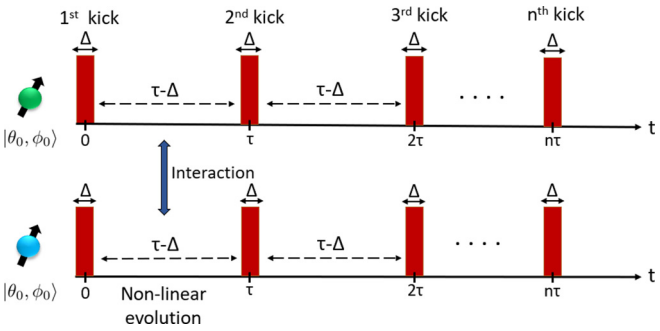

FIG. 1. Linear kicks and nonlinear evolutions for simulating a QKT using two qubits.

interval $\tau \gg \Delta$ (see Fig. 1):

$$H(t) = pJ_x, \text{ for } t \in \left[n\tau - \frac{\Delta}{2}, n\tau + \frac{\Delta}{2}\right] \text{ and}$$
$$H(t) = \frac{k}{2j\tau}J_z^2 \text{ otherwise.} \tag{1}$$

Here, $\mathbf{J} = [J_x, J_y, J_z]$ is the total angular momentum vector and $[n\tau - \frac{\Delta}{2}, n\tau + \frac{\Delta}{2}]$ describes the time lapse of the nth kick. The value of $\hbar$ has been set to 1. The nonlinear term describes a torsion about the z axis wherein k is the chaoticity parameter. Here, j is the total spin-quantum number. A spin-j QKT can be simulated using the symmetric subspace of $2j$ number of qubits. This property has earlier been used to study various quantum correlations [24]. In the case of $j = 1$ considered here, we need two interacting qubits. Further, we set $p\Delta = \pi/2$ for simplification of the quantum and classical maps [21,35]. The time evolution is governed by the Floquet unitaries

$$U_{\text{kick}} = e^{-i\frac{\pi}{2}J_x}, \; U_{\text{NL}} = e^{-i\frac{kJ_z^2}{2j}}, \text{ and } \; U_{\text{QKT}} = U_{\text{NL}}U_{\text{kick}}. \tag{2}$$

The overall unitary U_{QKT} is applied repeatedly to realize the desired number of kicks. In the Heisenberg picture, the evolution of the angular momentum operator for any time step is given by [21]

$$\mathbf{J}' = U_{\text{QKT}}^{\dagger}\,\mathbf{J}\,U_{\text{QKT}}. \tag{3}$$

The x and y components of $\mathbf{J}$ can be recast in the form of raising and lowering operators as $J_x = (J_+ + J_-)/2$ and $J_y = (J_+ - J_-)/2i$, which can then be studied in J_z eigenbasis $\{|m\rangle\}$ following the ladder equations

$$J_+|m\rangle = c_m|m+1\rangle \text{ and } J_-|m\rangle = d_m|m-1\rangle.$$

First let us consider the evolution of J_+ component since J_- will simply be its Hermitian conjugate (H.c):

$$J'_+ = U_{\text{QKT}}^{\dagger}J_+\,U_{\text{QKT}} = U_{\text{kick}}^{\dagger}U_{\text{NL}}^{\dagger}J_+\,U_{\text{NL}}U_{\text{kick}}. \tag{4}$$

Computing the action of U_{NL} on the operator in $|m\rangle$ basis,

$$\begin{aligned}\langle m|U_{\text{NL}}^{\dagger}J_+U_{\text{NL}}|n\rangle &= \langle m|e^{i\frac{k}{2j}J_z^2}J_+\,e^{-i\frac{k}{2j}J_z^2}|n\rangle \\ &= \exp\left\{i\frac{k}{2j}(m^2-n^2)\right\}\langle m|J_+|n\rangle \\ &= \exp\left\{i\frac{k}{2j}(m^2-n^2)\right\}c_n\delta_{m,n+1} \\ &= \begin{cases} e^{i\frac{k}{j}(n+\frac{1}{2})}c_n & \text{if } m = n+1, \\ 0 & \text{otherwise} \end{cases} \\ &= \langle m|J_+e^{i\frac{k}{j}(J_z+\frac{1}{2})}|n\rangle, \end{aligned} \tag{5}$$

so that

$$U_{\text{NL}}^{\dagger}J_+\,U_{\text{NL}} = J_+\,e^{i\frac{k}{j}(J_z+\frac{1}{2})}. \tag{6}$$

Next, the kick Floquet unitary has to be applied on the above operator. The action of the kick unitary is to bring about a clockwise rotation about the x axis by an angle of $\pi/2$ giving $U_{\text{kick}}^{\dagger}(J_x, J_y, J_z)U_{\text{kick}} = (J_x, -J_z, J_y)$, and hence

$$\begin{aligned}J'_+ = U_{\text{QKT}}^{\dagger}J_+\,U_{\text{QKT}} &= U_{\text{kick}}^{\dagger}J_+\,e^{i\frac{k}{j}(J_z+\frac{1}{2})}U_{\text{kick}} \\ &= (J_x - iJ_z)e^{i\frac{k}{j}(J_y+\frac{1}{2})}. \end{aligned} \tag{7}$$

The post-iteration transverse components of the angular momentum are thus

$$\begin{aligned}J'_x &= \frac{J'_+ + J'_-}{2} = \frac{1}{2}\left[(J_x - iJ_z)e^{i\frac{k}{j}(J_y+\frac{1}{2})} + \text{H.c}\right], \\ J'_y &= \frac{J'_+ - J'_-}{2i} = \frac{1}{2i}\left[(J_x - iJ_z)e^{i\frac{k}{j}(J_y+\frac{1}{2})} - \text{H.c}\right]. \end{aligned} \tag{8}$$

For the J_z operator, the nonlinear Floquet unitary brings about no change since it commutes with J_z. The only evolution of J_z is caused by $\pi/2$ rotation about the x axis giving $U_{\text{kick}}^{\dagger}J_zU_{\text{kick}} = J_y$, such that

$$J'_z = J_y. \tag{9}$$

In the next section, we will study the classical limit of the QKT.

Classical limit of QKT

It is insightful to first look into the classical features of the QKT in the semiclassical limit, i.e., $j \to \infty$. Expressing $X = J_x/j$, $Y = J_y/j$, and $Z = J_z/j$, one obtains $[X, Y] = iZ/j$, which vanishes in the large j limit. Under this classical limit, Eqs. (8) and (9) lead to the iterative map [21,35]

$$\begin{aligned}X' &= X\cos(kY) + Z\sin(kY), \\ Y' &= X\sin(kY) - Z\cos(kY), \\ Z' &= Y. \end{aligned} \tag{10}$$

These components can be parametrized in terms of the polar coordinates (θ, ϕ) as $X = \sin\theta\cos\phi$, $Y = \sin\theta\sin\phi$, and $Z = \cos\theta$. As the value of the chaoticity parameter k increases, the phase space undergoes a transition from a regular to a combination of regular and chaotic regions before becoming predominantly chaotic for large values of k. The classical phase space is shown for different values of k in Fig. 2. The trivial fixed points $(\theta, \phi) = (\pi/2, 0)$ and $(\pi/2, \pi)$ can be seen in Fig. 2(a), which become unstable at $k = 2$. At $k = 2$ new fixed points are born and they move away as k is increased as shown in Fig. 2(b). For large value of $k > 5$ the phase space becomes mostly chaotic as in Fig. 2(d).

III. QKT WITH A PAIR OF NMR QUBITS

We now return to the quantum case with a pair of NMR qubits. We consider a single QKT comprising a pair of qubits

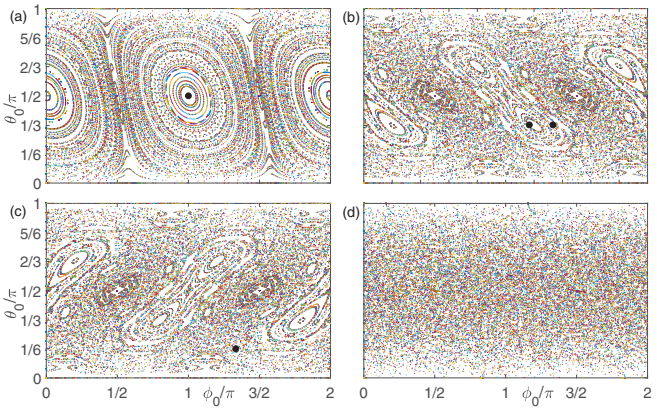

FIG. 2. Classical trajectories of the kicked top in $|\theta, \phi\rangle$ phase space for chaoticity parameter values (a) $k = 0.5$, (b) $k = 2.5$, (c) $k = -2.5$, and (d) $k = 2\pi + 2.5$. The phase space points chosen for detailed analysis are marked by black dots.

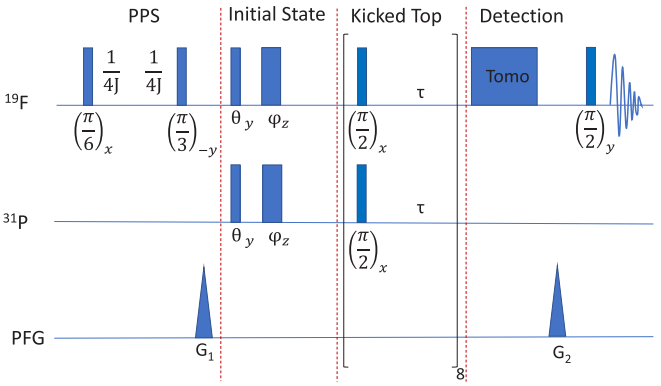

FIG. 3. NMR pulse sequence for simulating a QKT in a two-qubit system. The flip angles and phases (subscripts) are shown under each radio-frequency pulse. Here G_1 and G_2 correspond to pulsed-field-gradients (PFG).

with spin angular-momentum operators $\mathbf{I}_1$ and $\mathbf{I}_2$, respectively. By denoting the total z component $J_z = I_{z1} + I_{z2}$, we obtain the nonlinear term $J_z^2 = \mathbb{1}/4 + \mathbb{1}/4 + 2I_{z1}I_{z2}$. Dropping identities which only introduce global phases, we may realize the nonlinear dynamics using the bilinear term. Such an interaction naturally occurs in a pair of nuclear spins coupled via indirect spin-spin interaction under weak-coupling limit, i.e.,

$$H_{\mathcal{J}} = 2\pi\mathcal{J} I_{z1} I_{z2}. \tag{11}$$

Here $\mathcal{J}$ is the strength of the indirect spin-spin interaction. For a pair of heteronuclear spins, the Zeeman Hamiltonian terms can be ignored by moving on to a doubly rotating frame. Comparing the above Hamiltonian with the second term of Eq. (1), we obtain $k = 2\pi\mathcal{J}\tau$.

In our experiments, the pair of qubits was formed by ^{19}F and ^{31}P spins of sodium fluorophosphate dissolved in D_2O (5.3 mg in 600 μl). All experiments were performed on a 500 MHz Bruker NMR spectrometer at ambient temperatures and on-resonant conditions. The indirect spin-spin coupling $\mathcal{J} = 868$ Hz. The experiments consisted of two parts, i.e., preparation of the initial state (θ_0, ϕ_0), followed by simulating a QKT as illustrated in Fig. 1.

In NMR systems, owing to the low nuclear polarization at an ambient temperature T and a typical Zeeman field B_0, the initial thermal equilibrium state

$$\rho_0 = \frac{\mathbb{1}}{4} + \epsilon\tilde{\rho}$$

is highly mixed with a low purity factor $\epsilon \sim 10^{-5}$, which accounts for a finite nuclear magnetization. The uniform background population represented by identity remains invariant under unitary evolution, while the traceless deviation density matrix $\tilde{\rho} = I_{z1} + I_{z2}$ evolves and captures all the interesting dynamics. Preparing a pure state in an NMR system requires extremely low temperatures and unrealistically high magnetic fields. The standard protocol thus involves the preparation of a pseudopure state [36] which mimics pure state dynamics.

The NMR sequence for the entire QKT experiment is shown in Fig. 3. We utilize $\{|0\rangle, |1\rangle\}$ eigenbasis of I_z as the computational basis. We first prepare the $|00\rangle$ pseudopure state by transforming $\tilde{\rho}$ into $I_{z1} + I_{z2} + 2I_{z1}I_{z2}$ using a pair of radio-frequency pulses followed by a pulsed field gradient (PFG), which introduces a spatially inhomogeneous magnetic field across the sample volume, thereby destroying transverse components of the magnetization.

Subsequently, a θ_y pulse followed by a ϕ_z pulse (as shown in Fig. 3), initializes the qubits along a spin coherent state,

$$\rho_{\theta,\phi} \approx (1-\epsilon)\frac{\mathbb{1}}{4} + \epsilon[|\theta,\phi\rangle\langle\theta,\phi| \otimes |\theta,\phi\rangle\langle\theta,\phi|], \tag{12}$$

where

$$|\theta,\phi\rangle = \cos(\theta/2)|0\rangle + e^{i\phi}\sin(\theta/2)|1\rangle \tag{13}$$

is the corresponding Bloch vector for each qubit. The above initialization is analogous to the classical initialization of the kicked top into the (θ, ϕ) point on the phase space. The latter pulses for different ϕ angles were generated by an optimal control technique [37].

We now apply kicks via radio-frequency $(\pi/2)_x$ pulses with the Hamiltonian

$$H_{\rm rf} = \frac{\pi}{2\Delta}(I_{x1} + I_{x2}), \tag{14}$$

on both the qubits. Comparing with the first term in Eq. (1), we choose $\pi/(2\Delta) = p$. Here the pulse duration $\Delta \ll k/(2\pi\mathcal{J}) = \tau$, the duration of nonlinear evolution corresponding to the chaoticity parameter k (see Fig. 1). Thus in our experiment, $U_{\rm kick} = \exp(-iH_{\rm rf}\Delta)$, $U_{\rm NL} = \exp(-iH_{\mathcal{J}}\tau)$, and $U_{\rm QKT} = U_{\rm NL}U_{\rm kick}$ [see Eq. (2)].

We applied $U_{\rm QKT}$ for up to n times and estimated the ^{19}F reduced density operator $\rho_n = {\rm Tr}_{\rm P}[U_{\rm QKT}^n \rho_{\theta,\phi} U_{\rm QKT}^{n\dagger}]$ using single-qubit pure-phase quantum state tomography [38]. It consists of the following three NMR experiments: (i) A PFG to destroy all the coherences followed by a $(\pi/2)_y$ pulse to obtain the diagonal elements of the density matrix; (ii) $(\pi/2)_{-y}$ pulse followed by a PFG and $(\pi/2)_y$ pulse to obtain the real part of the off-diagonal coherence element; (iii) $(\pi/2)_{-x}$ pulse followed by PFG and $(\pi/2)_y$ pulse to obtain the imaginary part of the off-diagonal coherence element. This way one can reconstruct the single-qubit deviation density matrix $\tilde{\rho}_n$ from only pure-phase NMR signals which are easier to quantify. We

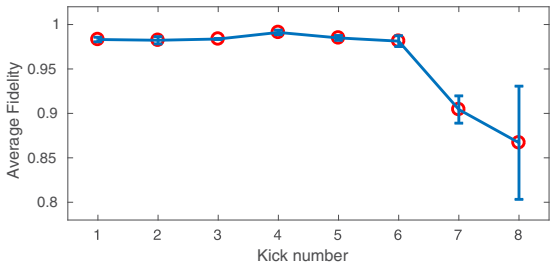

FIG. 4. Average fidelity of the experimental states for various kick numbers. The error bars indicate one standard deviation of distribution.

estimated the fidelity [39]

$$F\left(\tilde{\rho}_n, \tilde{\rho}_n^{\text{th}}\right) = \frac{\text{Tr}\left[\tilde{\rho}_n\, \tilde{\rho}_n^{\text{th}}\right]}{\sqrt{\text{Tr}\left[\tilde{\rho}_n^2\right]\text{Tr}\left[\left(\tilde{\rho}_n^{\text{th}}\right)^2\right]}} \tag{15}$$

of the n-kick experimental state $\tilde{\rho}_n$ with the corresponding theoretical deviation state $\tilde{\rho}_n^{\text{th}}$ for all initialization points (θ, ϕ) and for all k values. The average fidelity versus kick number displayed in Fig. 4 indicates high fidelities of above 0.95 up to six kicks and above 0.8 up to eight kicks.

A. Probing quantum chaos via von Neumann entropy

It has been observed that a kicked top in a state corresponding to a classically chaotic region results in higher entanglement production [18,21]. For an entangled pair of qubits, the reduced density matrix of either one has higher mixedness than the two-qubit composite state. Of course, since we are considering a closed quantum system, the dynamics is essentially unitary and entropy of the entire system remains invariant. However, the degree of entanglement, and hence the degree of chaos, can be quantified by the von Neumann entropy

$$S(\rho_n) = -\sum_{\lambda_\pm \neq 0} \lambda_\pm \log_2 \lambda_\pm \tag{16}$$

of the reduced density operator ρ_n with eigenvalues $\lambda_\pm = (1 \pm \epsilon\alpha_n)/2$. Here $\pm\alpha_n$ are eigenvalues of the traceless deviation part of ρ_n. However, in low-purity conditions, the von Neumann entropy is already close to unity,

$$S(\rho_n) \simeq 1 - \epsilon^2\alpha_n^2,$$

due to the dominant contribution of the identity term in ρ_n. Accordingly, the contrast between regular and chaotic regions is low. To address this issue, we define an n-kick order parameter

$$s_n = \frac{1 - \frac{1}{n}\sum_{m=1}^{n} S(\rho_m)}{\epsilon^2} \simeq \left\langle \alpha_n^2 \right\rangle, \tag{17}$$

which extracts information of only the deviation part after different durations of evolution, and hence is a convenient measure of chaos. Smaller values of the order parameter correspond to less regular behavior or higher chaoticity.

We carried out four sets of experiments for chaoticity parameter $k \in \{0.5, 2.5, 2\pi - 2.5, 2\pi + 2.5\}$. In each case, we performed experimental quantum state tomography and estimated the order parameter s_n for the number n of kicks ranging from 1 to 8. The contours in Fig. 5 display the experimental order parameter s_n for various values of n as well as k. The color background is provided to compare the experimental contours with numerically simulated values of the order parameter. In each case, we have also calculated the rms deviation δ between the experimental and the simulated values. There appears to be a general agreement between the experimental and the simulated values.

For one kick at $k = 0.5$ we observe almost uniformly high order parameter $s > 0.6$, while for other k values, we observe similar patterns with a pair of highly ordered regular islands. Gradually, with a larger number of kicks, the order parameter settles to a characteristic pattern that resembles the classical phase space except for $k = 2\pi + 2.5$. Ultimately, we see domains of regular islands corresponding to high order parameters for all k values. As expected, we observe overall high order parameters for the lowest k value On the other hand, for high k values, unlike the classical case which shows highly chaotic phase space, in the quantum scenario, the regular islands survive. This is due to the periodicity of the order parameter with respect to the chaoticity parameter, i.e., $s(k) = s(\text{mod}(k, 2\pi))$. This is evident from the similarity between the contours of columns 2 and 4 in Fig. 5 as well as from the reflection symmetry between the columns 2 (or 4) and 3. The periodicity of entropy distribution as a function of chaoticity parameter k and the number of qubits has been theoretically studied in detail in [32].

The results presented in Fig. 5 show clear distinction in values of order parameter between the regular and chaotic regions. The time-averaged order parameter for regular regions is higher than that of chaotic regions for all values of chaoticity parameter k. This in turn reinforces the fact that time-averaged entropy of regular regions is less than that of chaotic regions. Theoretical studies of von Neumann entropy in the deep quantum regime with mixed phase space [19,31] have shown that there are instances where entropy of initial states in regular regions leads to the generation of high entanglement. But its time average is shown to be less than that of the chaotic region [19] and this observation agrees with our NMR experiments. Hence, time-averaged entropy serves as a good witness for quantum chaos.

B. Husimi probability distribution

Although the von Neumann entropy captures the mixedness of the reduced density operator, it is not sensitive to its angular location on the Bloch sphere. The Husimi probability function measures overlap of the state ρ_n at any time with Bloch vectors $\{|\theta, \phi\rangle\}$ on the phase space and is given by [23]

$$\text{Q}_n(\theta, \phi, t) = \frac{1}{\pi}\langle\theta, \phi|\rho_n|\theta, \phi\rangle. \tag{18}$$

For a state initialized into a regular region, the Husimi probability distribution is either stationary or highly periodic. On the other hand, for a state initialized into a chaotic region, the distribution shows more intricate dynamics. The Husimi distributions for select values of k and initial states are shown in Fig. 6. Here the mesh-grid lines represent the experimental distribution while the color background represents the

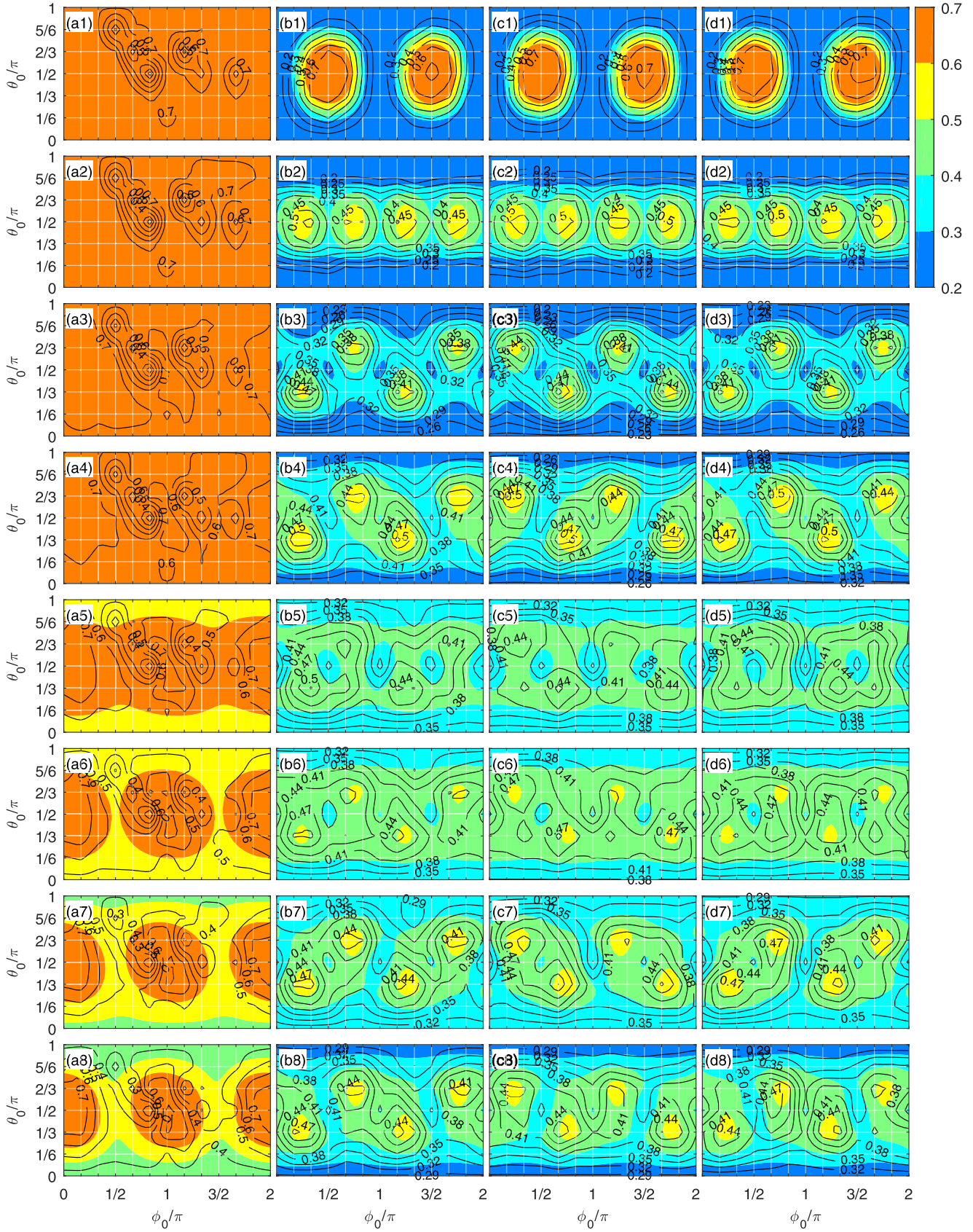

FIG. 5. Contours represent experimental order parameter averaged over n kicks (s_n) for chaoticity parameter $k = 0.5$ [(a1)–(a8)], $k = 2.5$ [(b1)–(b8)], $k = 2\pi - 2.5$ [(c1)–(c8)], and $k = 2\pi + 2.5$ [(d1)–(d8)]. Background color maps represent the corresponding simulated values. Average rms deviations $\langle\delta\rangle$ between the experimental and simulated values are 0.14 for $k = 0.5$, 0.033 for $k = 2.5$, 0.031 for $k = 2\pi - 2.5$, and 0.032 for $k = 2\pi + 2.5$.

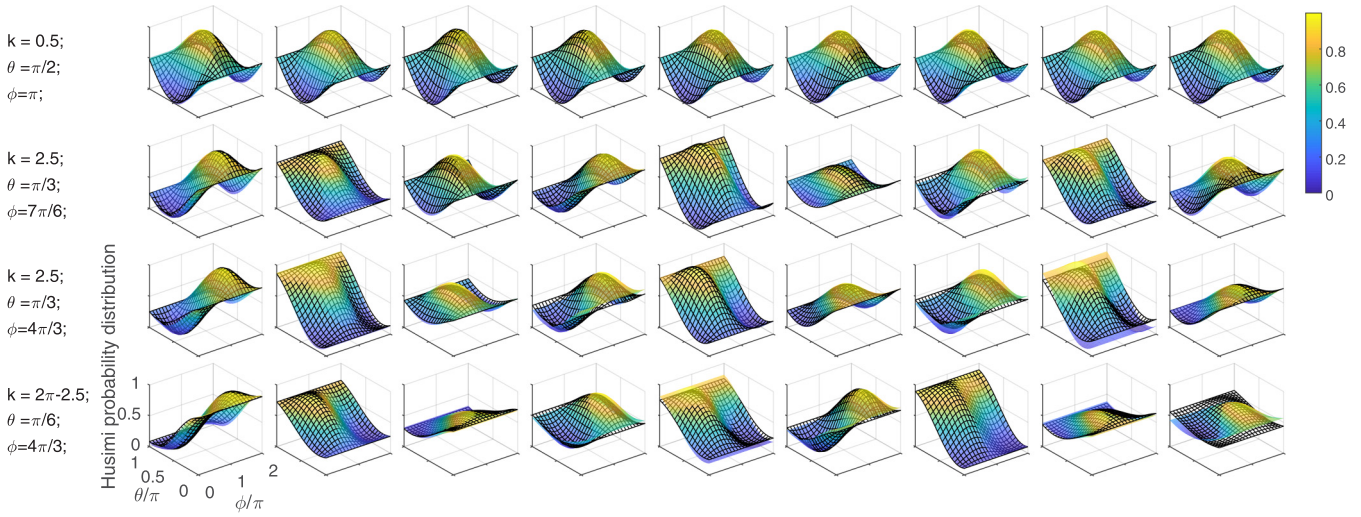

FIG. 6. Experimental (mesh grids) and simulated (color background) Husimi probability distributions (in units of $1/\pi$) for certain k values and initial states (as indicated in the left of each row) after kick numbers $n = 0$ to 8 (from left to right).

numerically simulated distribution. We see that the state $|\pi/2, \pi\rangle$ for $k = 0.5$ which lies in the high-order-parameter region is localized throughout the evolution time. On the other hand, states initialized to lower order-parameter regions undergo periodic temporal modulations and thus exhibit significant delocalization over the Bloch sphere.

To capture the delocalization better, we tracked the dynamics of the first 20 maxima of the Husimi probability distribution. As shown in Fig. 7, the maxima regions for $k = 0.5$ are localized after the evolution, whereas for higher values of k, the maxima regions spread out on the phase space. Interestingly, the mismatch between experiment and simulated data increases with increasing k, implying the sensitivity of the system dynamics to initial conditions and experimental imperfections. This observation reinforces the notion that quantum chaos could be a hurdle in quantum information processing tasks [17].

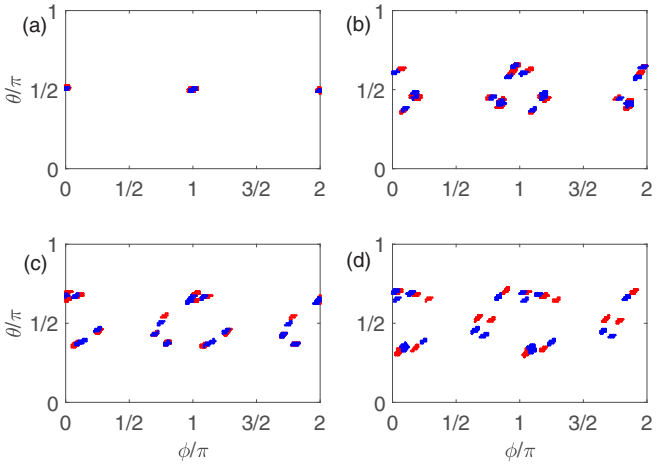

FIG. 7. Distribution of maxima neighborhood of Husimi probability function on the Bloch sphere. Blue dots represent simulated data and red dots represent experimental data for the values of k and initial angles (a) $k = 0.5$, $|\theta, \phi\rangle = |\pi/2, \pi\rangle$, (b) $k = 2.5$, $|\theta, \phi\rangle = |\pi/3, 7\pi/6\rangle$, (c) $k = 2.5$, $|\theta, \phi\rangle = |\pi/3, 4\pi/3\rangle$, and (d) $k = 2\pi - 2.5$, $|\theta, \phi\rangle = |\pi/6, 4\pi/3\rangle$.

IV. CONCLUSIONS

In this work, we have experimentally studied quantum signatures of classical chaos on a two-qubit NMR system using a kicked top model. We characterized the dynamics via two distinct ways:

(i) Correspondence to classical phase space was studied using order-parameter profiles extracted from the von Neumann entropy. These profiles showed not only good correspondence with the classical phase space for lower chaoticity parameters, but also the inherent periodicity and symmetry in the quantum dynamics for larger values of the chaoticity parameter. It is interesting to see such signatures in the NMR case where the quantum state purity is well below the threshold for entanglement.

(ii) The localization and delocalization of the quantum states on the Bloch sphere were characterized via the Husimi probability distribution. They also showed a temporal periodicity that is characteristic of the quantum system. We observed the localization of the profiles for low-chaoticity conditions and significant delocalization otherwise. In addition, the study also highlighted the sensitivity of the distribution to experimental imperfections particularly at higher values of chaoticity parameter.

The system considered here, being only two qubits, is deeply embedded in the quantum regime, but the marks of quantum chaos are nonetheless interesting. The NMR test bed should facilitate the possibility of extending such studies with a higher number of qubits. Further investigation of other quantum correlation measures such as discord, negativity, etc., will help us better understand the bridge between chaos in classical and in quantum systems.

ACKNOWLEDGMENTS

We acknowledge useful discussions with Prof. M. S. Santhanam, Sudheer Kumar, Deepak Khurana, and Soham

Pal. This work was partly supported by DST/SJF/PSA-03/2012-13 and CSIR 03(1345)/16/EMR-II. U.T.B. acknowledges the funding received from the Department of Science and Technology, India, under the scheme Science and Engineering Research Board (SERB) National Post Doctoral Fellowship (NPDF) File No. PDF/2015/00050.

[1] E. Ott, *Chaos in Dynamical Systems* (Cambridge University, Cambridge, U.K., 2002).
[2] S. Strogatz, *Nonlinear Dynamics and Chaos* (Perseus, New York, 2000).
[3] T. Kapitaniak, *Chaos for Engineers: Theory, Applications, and Control* (Springer-Verlag, Berlin, 2000).
[4] R. V. Jensen, Nature **355**, 311 (1992).
[5] S. Tomsovic and D. Ullmo, Phys. Rev. E **50**, 145 (1994).
[6] W. K. Hensinger, H. Haffner, A. Browaeys, N. R. Heckenberg *et al.*, Nature (London) **412**, 52 (2001).
[7] D. A. Steck, W. H. Oskay, and M. G. Raizen, Science **293**, 274 (2001).
[8] T. Graß, B. Juliá-Díaz, M. Kuś, and M. Lewenstein, Phys. Rev. Lett. **111**, 090404 (2013).
[9] S. Chaudhury, A. Smith, B. E. Anderson, S. Ghose, and P. S. Jessen, Nature **461**, 768 (2009).
[10] G. B. Lemos, R. M. Gomes, S. P. Walborn, P. H. S. Ribeiro, and F. Toscano, Nat. Commun. **3**, 1211 (2012).
[11] J. Larson, B. M. Anderson, and A. Altland, Phys. Rev. A **87**, 013624 (2013).
[12] C. Neill, P. Roushan, M. Fang, Y. Chen, M. Kolodrubetz, Z. Chen, A. Megrant, R. Barends, B. Campbell, B. Chiaro *et al.*, Nat. Phys. **12**, 1037 (2016).
[13] M. Bitter and V. Milner, Phys. Rev. Lett. **118**, 034101 (2017).
[14] E. V. H. Doggen, B. Georgeot, and G. Lemarié, Phys. Rev. E **96**, 040201 (2017).
[15] D. Wintgen and H. Friedrich, Phys. Rev. Lett. **57**, 571 (1986).
[16] A. G. Araujo-Ferreira, R. Auccaise, R. S. Sarthour, I. S. Oliveira, T. J. Bonagamba, and I. Roditi, Phys. Rev. A **87**, 053605 (2013).
[17] B. Georgeot and D. L. Shepelyansky, Phys. Rev. E **62**, 6366 (2000).
[18] X. Wang, S. Ghose, B. C. Sanders, and B. Hu, Phys. Rev. E **70**, 016217 (2004).
[19] M. Lombardi and A. Matzkin, Phys. Rev. E **83**, 016207 (2011).
[20] J. B. Ruebeck, J. Lin, and A. K. Pattanayak, Phys. Rev. E **95**, 062222 (2017).
[21] J. N. Bandyopadhyay and A. Lakshminarayan, Phys. Rev. E **69**, 016201 (2004).
[22] J. N. Bandyopadhyay and A. Lakshminarayan, Phys. Rev. Lett. **89**, 060402 (2002).
[23] F. Haake, H. Wiedemann, and K. Zyczkowski, Ann. Phys. (Berlin) **504**, 531 (1992).
[24] V. Madhok, V. Gupta, D.-A. Trottier, and S. Ghose, Phys. Rev. E **91**, 032906 (2015).
[25] F. Haake, *Quantum Signatures of Chaos,* 3rd ed. (Springer, Berlin, 2010).
[26] O. Bohigas, M. J. Giannoni, and C. Schmit, Phys. Rev. Lett. **52**, 1 (1984).
[27] T. Bhattacharya, S. Habib, and K. Jacobs, Phys. Rev. Lett. **85**, 4852 (2000).
[28] U. T. Bhosale and M. S. Santhanam, Phys. Rev. E **95**, 012216 (2017).
[29] M. Kumari and S. Ghose, Phys. Rev. E **97**, 052209 (2018).
[30] S. Dogra, V. Madhok, and A. Lakshminarayan, arXiv:1808.07741.
[31] M. Kumari and S. Ghose, arXiv:1806.10545.
[32] U. T. Bhosale and M. S. Santhanam, Phys. Rev. E **98**, 052228 (2018).
[33] D.G.Cory, R. Laflamme, E. Knill *et al.*, Fortschr. Phys. **48**, 875 (2000).
[34] I. S. Oliveira, T. J. Bonagamba, R. S. Sarthour, J. C. Freitas, and E. R. de Azevedo, *NMR Quantum Information Processing* (Elsevier Science, New York, 2007).
[35] F. Haake, M. Kus, and R. Scharf, Z. Phys. B **65**, 381 (1987).
[36] D. G. Cory, A. F. Fahmy, and T. F. Havel, Proc. Natl. Acad. Sci. USA **94**, 1634 (1997).
[37] N. Khaneja, T. Reiss, C. Kehlet, T. S. Herbruggen, and S. J. Glaser, J. Magn. Reson. **172**, 296 (2005).
[38] V. S. Anjusha and T. S. Mahesh, arXiv:1802.02792.
[39] E. M. Fortunato, M. A. Pravia, N. Boulant, G. Teklemariam, T. F. Havel, and D. G. Cory, J. Chem. Phys. **116**, 7599 (2002).